RSC Advances

ROYAL SOCIETY OF CHEMISTRY

www.rsc.org/advances

Self-stabilized Pt-Rh bimetallic nanoclusters as durable electrocatalyst for dioxygen reduction in PEM fuel cells

B. Narayanamoorthy [a], K.K.R. Datta[c], M. Eswaramoorthy[b] and S. Balaji [a,*]

[a]*Department of Chemistry, Faculty of Science, Sri Chandrasekharendra Saraswathi Viswa Mahavidyalaya (SCSVMV University), Enathur, Kanchipuram - 631 561, India.*

[b]*Nanomaterials and Catalysis Lab, Chemistry and Physics of Materials Unit, Jawaharlal Nehru Centre for Advanced Scientific Research (JNCASR), Bangalore – 560 064, India.*

[c]*Regional Centre of Advanced Technologies and Materials, Faculty of Science, Department of Physical Chemistry, Palacky University, 771 46 Olomouc, Czech Republic.*

[*] To whom correspondence should be addressed. Tel.: +91-44-27264293; fax: +91-44-27264285.

E-mail address: prof.balaji13@gmail.com (S. Balaji).

Abstract

The self-stabilized Pt-Rh nanoclusters (NC) were prepared by surfactant free chemical reduction method using formic acid as the reducing agent. The elemental composition was determined by EDX analysis. The synthesized cluster was used as a supportless (SL) electrocatalyst for the reduction of oxygen (ORR) in acid medium. The composition of Pt-Rh bimetal NC in terms of atomic weight percentage was optimized based on available electrochemical surface area. Hydrodynamic linear scan voltammetric profiles show that the onset potential for oxygen reduction is 0.78 V vs. RHE at the electrode rotation rate of 2400 rpm with 17.8 μg cm^{-2} loading of the SL Pt_3Rh exhibiting the limiting current density of 3.5 mA cm^{-2}. The durability of the electrocatalysts was investigated by performing the accelerated durability test (ADT) and found that the electrochemical surface area (ECSA) for SL Pt_3Rh has increased nearly by 9.2 % and at the same time retaining nearly 85 % of its initial limiting current density after 15,000 potential cycles. For comparison Vulcan carbon supported Pt_3Rh was synthesized under identical conditions and subjected to electrochemical investigation. Both supportless and VC supported Pt_3Rh NC electrocatalysts were found to follow a direct 4-electron transfer mechanism. In order to improve the activity, SL Pt@Pt_3Rh NC was synthesized and used as the catalyst. At 0.9 V, the mass activity (0.085 mA μg^{-1}) of the Pt@Pt_3Rh NC was found to be nearly 34 times compared to SL Pt_3Rh NC (0.0025 mA μg^{-1}). The present investigation concludes that the SL Pt_3Rh NC could be used as a potential electrocatalyst for ORR in sulfuric acid medium which possesses good stability compared to Pt based ORR catalysts reported in literature.

Keywords: *Pt-Rh nanoclusters; oxygen reduction; fuel cell; catalyst durability.*

1. Introduction

Till to date, the state of the art of designing/making of electrocatalysts are Pt and Pt based nanostructures for polymer electrolyte membrane fuel cells (PEMFC) to catalyze the cathodic reduction of molecular oxygen (ORR)[1]. The inherently sluggish kinetics of ORR is driving the search for finding the active and durable cathode electrocatalyst for PEMFC. During the initial development of fuel cells bulk Pt was employed as electrocatalyst. But, it suffered from the disadvantage of low surface area and under utilization. Later on, the nanoelectrocatalysts have got more attention due to their unique physical and chemical properties. The widely employed electrocatalyst is Pt nanoparticle supported on carbon black (Pt/C)[2, 3]. Therefore, when Pt/C is used as catalyst in PEMFCs an enhanced activity was observed due to the enhancement in electrochemical surface area (ECSA) and also increased mass and specific activities were obtained. This led to the development of commercial fuel cell stack systems and prototype models. In real PEMFCs, employment of different nano morphologies helped to reduce cathode catalyst (Pt) loading in membrane electrode assemblies from 0.4 mg cm^{-2} to 0.1 mg cm^{-2} to achieve the DOE target which aims to reduce the exorbitant cost of fuel cell components. But, the inherent disadvantage of real stack systems is the reduction in performance after several hours of operation. Because, the carbon surface undergoes oxidation and results in Pt nanoparticles agglomeration and leaching out from the surface and hence reducing the oxygen reduction kinetics and shortening the expected life span of the catalyst layer[4-6]. Although not cost effective Pt is highly preferred due to its high catalytic activity and resistant to oxidation in acid medium compared to most of the noble and non-noble metals[7-9]. Still Pt is not the front runner in newer catalyst materials in terms of stability.

Therefore, in order to improve the stability and to avoid the carbon corrosion issues, supportless bimetal nanostructures have been increasingly employed as durable electrocatalysts by many researchers. Sun et al., have reported the synthesis of highly durable multiarmed star like Pt nanowires as supportless electrocatalyst which retains ~90 % of its initial ECSA after 4,000 potential cycles[7]. Tan et al., have studied the durability of Au/Pt and Au/Pt_3Ni as self-supported electrocatalysts and observed 6.8 % and 9.9 % loss of ECSA after 5,000 potential cycles[8]. Wang et al., have shown that Pt nanoparticle netlike-assembly synthesized through a surfactant assisted hydrothermal method exhibited high durability and only 9 % loss in ECSA after 20,000 potential cycles[9]. Huang et al., have reported the synthesis of highly porous Pt_3Ni nanocrystals by PVP assisted method and found that 27.3 % of loss in ECSA after 6,000 potential cycles[10]. A mixed PtPdCu alloy nanoparticle nanotubes were prepared with Cu nanowire template assisted method and after 30,000 potential cycles nearly 20 % loss in ECSA with a negative shift in the half-wave potential of 5 mV was observed by Li et al.,[11]. Different successful strategies on bimetal electrocatalysts with enhanced stability were witnessed for ORR by a novel combination of Pt with the uncommon elements like Rh, Re, Os, etc.[12-14].

Nearly three decades ago, bulk PtRh alloy was employed as binary electrocatalyst for small alcohol oxidations and found to exhibit improved catalytic activity than pure Pt[15-17]. Although Rh by itself is not catalytically active, many attempts have been reported over the influence of Rh nanoparticles on the catalytic activity of Pt for the breaking of C-C and C-H bonds during the oxidation of small organic molecules for fuel cell applications[18-21]. Park et al., have studied the catalytic activity of PtRh and PtRuRhNi alloy nanoparticles using single cell system for methanol oxidation reaction (MOR) and concluded that the presence of Rh may influence the surface regeneration of active Pt surface. They have investigated the ORR activity

without much attention on stability[22, 23]. Noto et al., reported the carbon nitride supported PtRh prepared by pyrolysis method and discussed the ORR activity in acid medium[12, 24]. Friebel et al., have characterized the stability of PtRh (111) nanoparticles through an *in-situ* X-ray absorption spectroscopy (XAS) for ORR[25]. More recently Baraldi et al., have theoretically predicted that PtRh (111) bimetallic nanoclusters could enhance the chemical reactivity of the catalyst in fuel cell reactions[26]. Yuge et al., have reported the electronic structure and stability of PtRh nanoparticles analyzed by first principle calculations and predicted that PtRh alloy nanoparticles could function as a potential electrocatalyst for PEM fuel cells based on the observation of down shift of Pt d-band center in PtRh alloy[27].

The objectives of the present investigation were to synthesize the PtRh nanocluster morphology and to evaluate the electrocatalytic activity and stability for oxygen reduction reaction in acid medium by cyclic voltammetry in a standard three electrode electrochemical cell. The supportless Pt-Rh nanocluster electrocatalyst was prepared by chemical reduction method using formic acid without using any additional template and unambiguously characterized by X-ray diffraction (XRD), field emission scanning electron microscope (FESEM), high resolution transmission electron microscope (HRTEM) and energy dispersive X-ray analysis (EDX) to determine the size, shape, distribution and composition. The Pt-Rh composition (at. wt. %) was optimized based on the electrochemical activity towards oxygen reduction. For comparison Vulcan carbon (VC) supported electrocatalyst was synthesized under identical conditions and used for electrochemical investigations. The kinetic and thermodynamic parameters for ORR were calculated for both supportless and carbon supported Pt-Rh nanoclusters and the stabilities were evaluated under continuous potential cycling.

2. Experimental methods

2.1. Materials

Hexachloroplatinic acid (H_2PtCl_6. $6H_2O$), Rhodium (III) chloride monohydrate ($RhCl_3$. H_2O) were obtained as Pt and Rh metal precursors respectively from Sigma-Aldrich. Formic acid (98 %, Sigma) was used as reducing agent. For carbon supported catalysts, Vulcan carbon XC-72 (VC) was used as received from Cabot (I) Ltd as complementary pack. Nafion perfluorinated polymer resin solution (5 wt. %, Sigma-Aldrich) was applied as the catalyst binder, Sulfuric acid (Rankem), Methanol (98 %, Merck) and Absolute Ethanol (Merck) were all used as received. For all the solutions preparations Millipore (18 MΩ cm) water was used.

2.2. Preparation of Pt-Rh nanoclusters

Supportless Pt-Rh nanoclusters (SL Pt-Rh NC) were synthesized by slow reduction method by the following procedure. Briefly, 20 mL of an aqueous solution containing 24 mg of H_2PtCl_6. $6H_2O$ and 6 mg of $RhCl_3$. H_2O (3:1 Pt-Rh atomic wt. %) was taken in a beaker and 1 mL of formic acid was added and the mixture was kept aside undisturbed for 72 h at room temperature. The mixture was centrifuged at 8,000 rpm and washed with water and methanol for several times. Finally, the product was collected and dried in an air oven at 80 °C. The atomic ratio of Pt and Rh was varied as 3:1, 1:1 and 1:3. The carbon supported catalysts were prepared by adding 7.5 mg of VC at the initial stage of above synthesis procedure before adding the reducing agent. Also, the supportless Pt@Pt_3Rh NC was synthesized by adding Pt precursor over the previously synthesized Pt-Rh (3:1) NC and further reducing with formic acid for another 72 h to obtain Pt skin over Pt_3Rh.

2.3. Characterization techniques

The as prepared supportless and carbon supported Pt-Rh NC electrocatalysts were characterized by XRD (Bruker-D8 diffractometer using Cu-K_α radiation, λ=1.54 Å, current: 30 mA and voltage: 40 kV) FESEM and EDX mapping (FEI instruments, Nova-Nano SEM-600, Netherlands). TEM and HRTEM images were obtained by re-dispersing the catalyst sample in absolute ethanol by sonication and drop casting on a carbon-coated copper grid (FEI Tecnai 30G2, 300 kV).

Typically, the catalyst ink was prepared by dispersing 0.5 mg of catalyst in 1 mL of absolute ethanol and ultrasonicating for 3 min to get a homogeneous dispersion. Then, 7 µl of catalyst ink was pipetted out on to a mirror finished surface of the rotating disc glassy carbon working electrode (GC-RDE, 5 mm) to obtain a metal loading of about 17.8 µg cm^{-2} for both supportless and supported electrocatalysts, which was subsequently covered by 5 µl of 0.05 wt. % Nafion. The indicated metal loading of each catalyst is actually the sum of Pt and Rh. Prior to coating, the GC surface was polished with 0.05 µm alumina slurry, washed with ethanol and water and then subjected to ultrasonic agitation for 5 min in deionized water. For preliminary cyclic voltammetric investigations the catalyst loading of 40.8 µg cm^{-2} (15 µl) was maintained for all the compositions of Pt-Rh.

The electrochemical behavior of prepared Pt-Rh nanoclusters was investigated by CV and LSV techniques. The cyclic voltammograms were recorded in N_2 saturated 0.5 M H_2SO_4 at a sweep rate of 0.1 V s^{-1} between -0.1 to 1.2 V vs. RHE at 25 °C. The ORR polarization curves (LSV) were obtained in an O_2-saturated 0.5 M sulfuric acid solution at a sweep rate of 0.01 V/s and at the electrode rotation rates of 400, 800, 1200, 1600, 2000 and 2400 rpm using a rotator set up (Pine) interfaced with the potentiostat and controlled through NOVA 1.9 software (Autolab).

The standard model of double jacketed electrochemical cell was employed for three electrode configuration. The electrolyte was maintained at the required temperature by circulating water in the outer jacket using a thermostat (Equibath, India). The counter electrode used was a plain Pt sheet (1 cm^2) and double-junction Ag/AgCl filled (saturated KNO_3) was used as reference electrode. All the potential values are reported to reversible hydrogen electrode (RHE) by adding 0.21 V to the obtained potential values[28]. The long term stability of Pt-Rh electrocatalysts was checked by the accelerated durability test (ADT) i.e., by applying continuous potential cycles to the working electrode between 0.6 and 1.2 V in O_2-saturated 0.5 M H_2SO_4 solution at 25 °C, at the scan rate of 0.1 V s^{-1} and recording both CV and LSV patterns during the experiment for every 1,000 cycles.

3. Results and discussion

3.1. XRD, SEM and TEM results

The powder XRD patterns of both supportless and VC supported Pt_3Rh NC are shown in Fig. 1. From the XRD patterns we observed that, both the catalysts show a face centered cubic structure with the characteristic peaks at the diffraction angles (2θ): 40.4°, 47.0°, 68.7° and 82.1° corresponding to the (111), (200), (220) and (311) crystalline planes respectively. The 2θ of the (111) peak for both SL Pt_3Rh (Fig. 1a) and Pt_3Rh /VC (Fig. 1b) is slightly shifted to a higher angle by 0.6° compared to pure Pt (2θ=39.8°) respectively. The same trend was also observed in 2θ values of the (200), (220) and (311) peaks. The higher angle shift confirms the alloy formation between Pt and Rh (incorporation of Rh atoms into the fcc lattice of Pt)[29], in both SL Pt_3Rh (Fig. 1a) and Pt_3Rh /VC (Fig. 1b) catalysts. In VC supported catalyst an additional peak observed at 2θ=23.8° shows the plane of hexagonal structure of conducting carbon substrate[30].

The average particulate size of the nanocrystals were estimated from XRD pattern using Debye-Scherrer equation and found to be ~ 4 nm for both the catalysts. The FESEM images of (ESI, Figs. S1a & S1b) supportless Pt_3Rh nanoclusters and (ESI, Figs. S1c & S1d) VC supported Pt_3Rh are shown in ESI, Fig. S1. It can be clearly observed that the supportless catalyst possesses cluster morphology composed of tiny nanoparticles. A uniform distribution without segregation was found from the FESEM images (ESI, Figs. S1c & S1d) of VC supported Pt_3Rh catalyst. The EDX pattern of SL Pt_3Rh is shown in ESI, Fig. S2a and the atomic wt. % composition of Pt and Rh were found to be 76.9 and 23 respectively with the expected stoichiometric ratio of nearly 3:1. Also, the elemental mapping clearly depicts (ESI, Figs. S2b-S2d), the homogenous distribution of Pt and Rh throughout the structure of supportless Pt_3Rh. The TEM images of the supportless electrocatalyst (Figs. 2a and 2b) confirm the assembly of smaller nanoparticles (less than 5 nm). The fine lattice fringes of nanoclusters (Fig. 2c) confirm the crystalline nature of Pt_3Rh bimetal nanoclusters. From the histogram (Fig. 2d) of the TEM image, the average particle size was found to be 3.3 nm with the standard deviation of around 0.74 nm and well correlates with the calculated average particle size from XRD pattern.

3.2. Optimization of Pt-Rh ratio

Cyclic voltammograms of SL Pt-Rh NC with different atomic ratios of Pt and Rh such as 3:1, 1:1 and 1:3 were recorded in N_2 saturated 0.5 M sulfuric acid between 0.0 and +1.2 V at 25 °C and shown in ESI, Fig. S3a. The ECSA of the metal nanocatalyst was determined by integrating the charges measured upon desorption/adsorption of hydrogen 'under potential deposition (H_{upd}) region' between -0.1 and 0.21 V. The electrochemically active surface areas of SL Pt-Rh NCs for all the three compositions were calculated and found that SL Pt-Rh 3:1

catalyst has the highest ECSA of 154.4 m^2 g^{-1} and this value is nearly 1.3 times higher than 1:1 (85.2 m^2 g^{-1}) and 3 times higher than 1:3 (43.1 m^2 g^{-1}) compositions. The higher magnitude of ECSA for SL Pt-Rh NC was comparable with the reported Pt-Ru/C (103.5 m^2 g^{-1}) bimetallic ORR electrocatalyst [31]. Also, the ECSA of 3:1 SL Pt-Rh was higher than those reported for 3D-PtRh alloy nanoporous and PtRh/carbon nitride catalysts[15, 27, 32]. Generally the observed higher surface areas of SL Pt-Rh electrocatalysts can be attributed to the fine structure of nanocluster morphology of Pt stabilized with Rh. From the CVs, it can be clearly observed that the metal-oxide reduction peak for 3:1 SL Pt-Rh shows a well defined reduction peak (0.52 mV) with positively shifted peak potential compared to the other two compositions.

The catalytic activity of SL Pt-Rh NC towards the dioxygen reduction was investigated by observing the reduction half cell profiles in O_2 saturated 0.5 M sulphuric acid under hydrodynamic conditions. Linear scan voltammograms were recorded for all the three compositions and compared in ESI, Fig. S3b. A higher limiting current density of 3.92 mA cm^{-2} was obtained for 3:1 SL Pt-Rh NC with an earlier onset potential and by magnitude 100 to 150 mV higher than the other two compositions investigated. The exchange current density, transfer coefficient and the onset potential values were obtained from the corresponding Tafel plots and given in ESI, Table S1 (ESI, Fig. S4a). A positive shift of half-wave potential ($E_{1/2}$) was observed for 3:1 SL Pt-Rh NC by 40-200 mV compared to 1:1 and 1:3 ratios indicating the good catalytic activity of 3:1 SL Pt-Rh nanocluster for oxygen reduction.

The number of electrons transferred (n) during oxygen reduction was calculated from the corresponding K-L plots and found to be 4.0 for 3:1 SL Pt-Rh composition (ESI, Fig. S4b). The other two compositions of SL Pt-Rh (1:1 and 1:3) follow only two electron transfer mechanism with 'n' values of 2.7 and 2.6 respectively. It clearly depicts that the 3:1 SL Pt-Rh NC

electrocatalyst follows the most favorable electron transfer pathway and hence for further investigations this optimized composition was used. Also, the documented reports on Pt-Rh indicate that 20-30 atomic wt. % of Rh in Pt could be an optimized composition for fuel cell applications coinciding with our observation[12, 14, 18].

3.3. Cyclic voltammograms of Pt_3Rh nanoclusters

Fig. 3 shows the CVs of SL Pt_3Rh and VC supported Pt_3Rh nanoclusters recorded in N_2 saturated 0.5 M H_2SO_4 between 0.0 and +1.2 V at 25 °C. A sharp H-desorption peak was seen during the anodic sweep for both supportless and VC supported Pt_3Rh NC in the potential region between -0.1 and 0.18 V. The oxide formation peak in the anodic sweep indicates both the Pt-O and Rh-$O(OH)_3$ have formed between 0.7 and 1.1 V for both the catalysts and it is similar to the observed behavior in reported literature[18]. The SL Pt_3Rh NC has higher ECSA of 154.4 m^2 g^{-1}, which is nearly 2.5 times higher than Pt_3Rh/VC (63.11 m^2 g^{-1}) and nearly 45 times higher than Pt-black (Hispec-1000, JM) catalyst (5.9 m^2 g^{-1})[33] and comparable to the reported Pt-M alloy electrocatalysts[31, 34]. The larger ECSA of SL Pt_3Rh NC might be due to the larger exposed availability of active Pt sites and the lesser magnitude of VC supported Pt_3Rh catalyst might be due to the partially buried Pt active sites into the carbon support and also to the surface masking by CO formed (by oxidation of carbon substrate) over Pt active sites during the positive potential sweep[35].

3.4. Kinetics of ORR on Pt_3Rh nanoclusters

Fig. 4a shows the LSV of SL Pt_3Rh and Pt_3Rh/VC NC recorded in O_2 saturated 0.5 M H_2SO_4 at 2400 rpm. It can be seen that the supportless Pt_3Rh has more positive onset potential of

0.78 V nearly 40 mV higher than the VC supported Pt_3Rh (0.74 V) and a higher half-wave potential of 0.59 V was found for SL Pt_3Rh compared to 0.52 V for Pt_3Rh/VC showing the improved activity of the supportless Pt_3Rh electrocatalyst. But, we observed that, there is not much variation in the magnitude of observed limiting current density (j_L) values at 0.2 V for SL Pt_3Rh (3.50 mA cm^{-2}) and Pt_3Rh/VC NC (3.34 mA cm^{-2}). In order to estimate the magnitude of diffusional resistance offered by the electrolyte for the movement of oxygen molecules towards the electrodes surface, the limiting current density values were measured at different electrode rotation rate. As the rotation rate was increased from 400 to 2400 rpm the current density values also have increased from 1.94 to 3.50 mA cm^{-2}.

The number of electrons transferred (n) per oxygen molecule during the reduction of dioxygen was calculated from the corresponding Koutecky-Levich (K-L) plots (j_L^{-1} and $\omega^{-1/2}$) (Fig. 4b). From the K-L plots, the slope values were found to be 11.3 for SL Pt_3Rh and 12.46 for Pt_3Rh/VC and the corresponding 'n' values were found to be 4.0 and 3.5 respectively. It clearly shows that both the supportless and VC supported Pt_3Rh catalysts predominantly follow the direct 4-electron transfer mechanism during ORR. The kinetic current density for SL Pt_3Rh was calculated and found to be 0.08 mA cm^{-2} which is nearly 7 times higher than Pt_3Rh/VC (0.01 mA cm^{-2}). The mass activity (MA) of the electrocatalysts at 0.9 V was calculated by dividing the current density with catalyst loading (17.8 μg cm^{-2}) at 2400 rpm and found that the SL Pt_3Rh possesses 0.0025 mA μg^{-1}. This value is comparatively higher than VC supported Pt_3Rh and also comparable to some of the reported Pt/C[11] and some of the Pt nanostructures catalyzed ORR[36].

The mass transfer corrected Tafel plots were constructed for SL Pt_3Rh and Pt_3Rh/VC catalysts (ESI, Fig. S5) and the corresponding Tafel slope values were found to be 115 and 109 mV dec^{-1} for SL Pt_3Rh and Pt_3Rh/VC respectively. The obtained Tafel slope value is near to 120 mV dec^{-1}

corresponding to the clean Pt surface as reported for unsupported Pt black[37] and suggesting that the surface properties are quite similar to that of clean Pt surface. This clearly indicates the first electron transfer is the rate-limiting step during the reduction of dioxygen[1,35]. The ORR kinetic parameters such as half-wave potential ($E_{1/2}$); kinetic current density (j_k); kinetic rate constant (k); Tafel slope (b); electron transfer co-efficient (α); exchange current density (i_0) and mass activity at 0.9 V for both supportless and VC supported Pt_3Rh NC were calculated and summarized in Table 1. It can be clearly seen that the SL Pt_3Rh possesses better oxygen reduction activity than Pt_3Rh/VC in acid medium.

3.5. Accelerated durability tests of Pt_3Rh nanoclusters

The electrochemical stability of supportless and VC supported Pt_3Rh nanocluster electrocatalysts was investigated by ADT potential cycling. The catalyst coated GC-RDE working electrode was subjected to continuous potential cycling between 0.6 and 1.4 V at 25 °C in O_2 saturated 0.5 M H_2SO_4. During the potential cycling, the CVs were recorded with N_2 purging and LSVs were recorded with O_2 purging for every 1,000 potential cycles and the performance of the electrocatalysts was then compared in terms of normalized ECSA and ORR limiting currents. The ADT-CVs for SL Pt_3Rh (Fig. 5a) and Pt_3Rh/VC (ESI, Fig. S6a) electrocatalysts recorded at different intervals up to 15,000 cycles. As the potential cycling was continued the following changes were observed. (i) the hydrogen adsorption/desorption regions became more distinct and visibly developed, (ii) the shape of anodic Pt-oxide region attains the standard pattern as that of pure Pt, (iii) the cathodic reduction peak shifted more positively by 85 mV and (iv) the capacitance current has reduced nearly by 2.5 times from the initial value. During the ADT test, the micro structural changes of supportless Pt_3Rh nanoclusters through Rh

leaching was clearly observed from the continuously changing CV pattern during potential cycling which finally evolves and seem to be similar to the CV pattern of polycrystalline Pt. The dissolution of Rh from the SL Pt-Rh cluster morphology could increase the availability of Pt active sites and hence the ECSA was found to be higher after long term potential cycling. At the end of 15,000 cycles, the ECSA of SL Pt_3Rh was found increased from 154.4 to 168.2 m^2 g^{-1} while for Pt_3Rh/VC the ECSA has decreased from 63.1 to 6.2 m^2 g^{-1} i.e., nearly 9.2 % increase in ECSA was seen for SL Pt_3Rh whereas for VC supported Pt_3Rh almost 91.5 % of ECSA loss was observed.

Figs. 5b shows the ORR polarization curves recorded for SL Pt_3Rh and ADT potential cycling at various intervals. The ADT-LSV curves reveal that the SL Pt_3Rh NC (Fig. 5b) has retained nearly 85 % of its initial limiting current density with 14 mV positive shifts in half-wave potential with same onset potential. Whereas for Pt_3Rh/VC (ESI, Fig. S6b) nearly 61 % of its initial limiting current has decreased after 15,000 potential cycles and also the half-wave potential (80 mV) shifted more negatively increasing the overvoltage for dioxygen reduction. This could be due to the carbon support oxidation and the subsequent effects like catalyst dissolution and surface poisoning by CO adsorption (produced from carbon substrate oxidation) as reported in literatures[5, 6]. In the mixed kinetic-diffusion control region (0.9 to 0.65 V), it is obvious that the polarization curves of SL Pt_3Rh NC show 14.9 % current drop after the ADT, while there is a significant reduction of 60.6 % for the Pt_3Rh/VC. From ADT-CVs (ESI, Fig. 6c), the percentage of normalized ECSA and the loss of ORR current densities from ADT-LSVs (Fig. 5c) obtained at different intervals of potential cycling to assess the performance of the electrocatalysts. Table 2 shows the comparison of loss in ECSA and loss in ORR limiting current density for SL Pt_3Rh and Pt_3Rh/VC with the reported Pt based nanostructures either in

supportless or carbon supported (commercial Pt/C) catalysts from various literature reports[34-45]. It could be observed and concluded that the presence of Rh not only helps to stabilize the Pt nanoclusters but also affect the oxygen binding and desorption kinetics due to the improved electronic effects of Pt-Rh nanoalloy. The synergistic effect of bimetallic catalysts possessing an enhanced catalytic activity could be due to the following influencing factors: bi-functional nature, 'electronic' ligand effects and the change in inter-atomic distance, shift in d-band position and surface segregation[46-48].

Figs. 6a and 6b show the TEM images of SL Pt_3Rh NC recorded before and after ADT potential cycling (15,000 cycles) respectively. From these images, it can be clearly observed that there was no appreciable change in cluster morphology of bimetal catalyst and also from the corresponding histograms (Figs. 6c and 6d), the average particle size was found increased nearly by ~ 1.5 nm after 15,000 continuous potential cycles. It can be concluded that the SL Pt_3Rh NC electrocatalyst possesses an improved stability which is comparatively higher than VC supported Pt_3Rh and the reported PtRh/C by Sethuraman et al., (~77 % loss of ECSA after 20,000 potential cycles)[36]. These findings demonstrate that the nanocluster morphology of SL Pt_3Rh with the optimized composition of 3:1 possesses higher accessible active sites due to the presence of Rh and Rh-oxides as predicted by theoretical calculations reported by Friebel et al.,[25] and Baraldi et al.[26] and our finding offers the substantial experimental evidence.

3.6. Enhanced activity of Pt @ Pt_3Rh nanoclusters

Although the stability of SL Pt_3Rh was substantially improved compared to the standard Pt/C catalyst still the onset potential and activity need to be improved. Therefore, a thin layer of Pt was produced over the surface of previously formed SL Pt_3Rh, by reducing Pt precursor with

formic acid under the same conditions as before. The obtained catalyst is labeled as SL Pt@Pt_3Rh. The increase in Pt content was confirmed by EDX analysis (ESI, Fig. S7b) and the SEM and TEM images have (ESI, Fig. S7a) revealed the retention of cluster morphology without significant change. The CV profile of SL Pt@Pt_3Rh in N_2 saturated 0.5 M H_2SO_4 at a scan rate of 0.1 V s^{-1} is shown in ESI, Fig. S7c. It is seen that the peak potential of oxygen reduction is shifted more positively by 150 mV compared to SL Pt_3Rh. But the LSV profiles (ESI, Fig. S7d) at different rotation rates show an increased resistance as inferred from the sloppy behavior instead of a steep increase in cathodic current as expected for an active catalyst material and the current density goes on increasing slowly without reaching the limiting plateau. When ADT was performed over SL Pt@Pt_3Rh (Figs. 7a & 7b), nearly the same trend in stability up to 15,000 potential cycles was observed as that of SL Pt_3Rh. In conclusion, on further enriching the surface with a layer of Pt resulted in improved onset potential by 140 mV (ESI, Fig. S8) compared with SL Pt_3Rh but activity limitation was seen in the form of sloppy LSV behavior which might have resulted due to the smooth surface of Pt skin covering the rough surface structure and kinks of SL Pt_3Rh which are ideal sites for oxygen binding.

4. Conclusion

In the present work we have investigated the synthesis of Pt-Rh nanoclusters using formic acid as the reducing agent. TEM results shown that the average nanoparticle size was found to be ~ 4 nm finely distributed and the shift in 2θ value substantiates alloy formation between Pt and Rh. The synthesized electrocatalyst showed good activity towards oxygen reduction and the atomic composition between Pt and Rh was optimized based on the electrochemical performance in sulfuric acid medium. The optimum composition of Pt and Rh

was found to be 76.9 and 23 (atomic wt. %) showed the highest activity. The number of electrons transferred per mole of oxygen was found to be 4.0 for SL Pt_3Rh indicating that the reduction follows a 4-electron transfer mechanism. Accelerated durability tests shown that that SL Pt_3Rh exhibits the highest stability of 15,000 potential cycles with only 9.2% increase in ECSA and retained the ORR limiting current by 85 %. An attempt was made to further increase the activity part of Pt-Rh through the formation of Pt skin over the optimized composition of Pt_3Rh and this has in fact increased the mass activity nearly 34 times compared to SL Pt_3Rh NC and possessing nearly the same stability up to 15,000 cycles. To conclude, the presence of Rh in Pt_3Rh bimetal nanocluster morphology enhances the catalytic activity and provides considerable stability to Pt and seems to be the promising electrocatalyst for oxygen reduction in acid medium for PEM fuel cells.

Acknowledgement

This work was financially supported by the Board of Research in Nuclear Sciences (BRNS), Department of Atomic Energy (DAE), Govt. of India, under Basic Sciences program through sanction No. 2009/37/29/BRNS. S.B. profoundly thanks the management of SCSVMV University for having funded and created the necessary laboratory facilities to carry out this research project. B.N. thanks the CSIR, New Delhi for the award of Senior Research Fellowship (SRF) through the Sanction No. 09/1104(0001)/2013-EMR-I. K. K. R. Datta acknowledges financial support by the Operational Program Research and Development for Innovations-European Regional Development Fund (project CZ.1.05/2.1.00/03.0058 of the Ministry of Education, Youth and Sports of the Czech Republic) and the Operational Program Education for

Competitiveness-European Social Fund (project CZ.1.07/2.3.00/30.0004 of the Ministry of Education, Youth and Sports of the Czech Republic).

References

1. N.M. Markovic, T.J. Schmidt, V. Stamenkovic, P.N. Ross, *Fuel Cells*, 2001, **1**, 105.

2. H. Yano, E. Higuchi, H. Uchida, M. Watanabe, *J. Phys. Chem. B*, 2006, **110**, 16544.

3. Y.H Shih, G.V. Sagar, S.D. Lin, *J. Phys. Chem. C*, 2008, **112**, 123.

4. Y.S. Horn, W.C. Sheng, S. Chen, P.J. Ferreira, E.F. Holby, D. Morgan, *Top Catal*., 2007, **46**, 285.

5. K.H. Kangasniemi, D.A. Condit, T.D. Jarvi, *J. Electrochem. Soc*. 2004, **151**, E125.

6. J. Wang, G. Yin, Y. Shao, S. Zhang, Z. Wang, Y. Gao, *J. Power Sources*, 2007, **171**, 331.

7. S. Sun, G. Zhang, D. Geng, Y. Chen, R. Li, M. Cai, X. Sun, *Angew. Chem. Int. Ed*. 2011, **50**, 422.

8. Y. Tan, J. Fan, G. Chen, N. Zheng, Q. Xie, *Chem. Commun*. 2011, **47**, 11624.

9. Z. Xu, H. Zhang, H. Zhong, Q. Lu, Y. Wang, D. Su, *Appl. Catal. B*, 2012, **111-112**, 264.

10. X. Huang, E. Zhu, Y. Chen, Y. Li, C.-Yi Chiu, Y. Xu, Z. Lin, X. Duan, Y. Huang, *Adv. Mater*. 2013, **25**, 2974.

11. H.H. Li, C.H. Cui, S. Zhao, H.B. Yao, M.R. Gao, F.J. Fan, S.H. Yu, *Adv. Energ. Mater*. 2012, **2**, 1182.

12. V.D. Noto, E. Negro, K. Vezzu, L. Toniolo, G, Pace, *Electrochim. Acta*, 2011, **57**, 257.

13. D. Yoo, C. Pak, S.-Ah Jin, K.H. Lee, US pat., 13 710 173, 2013.

14. M.T. Reetz, M. Lopez, W. Grunert, W. Vogel, F. Mahlendorf, *J. Phys. Chem. B*, 2003, **107**, 7414.

15. D.F.A. Koch, D.A.J. Rand, R. Woods, *J. Electroanal. Chem*., 1976, **70**, 73.

16. P.N. Ross, K. Kinoshita, A.J. Scarpellino, P. Stonehart, *Electroanal. Chem. Interr. Electrochem*. 1975, **59**, 177.

17. N.R. De Tacconi, J.M. Leger, B. Beden, C. Lamy, *J. Electroanal. Chem*., 1982, **134**, 117.

18. F.H.B. Lima, D. Profeti, M. Chatenet, D. Riello, E.A. Ticianelli, E.R. Gonzalez, *Electrocatal*. 2010, **1**, 72.

19. T. Kawaguchi, Y. Rachi, W. Sugimoto, Y. Murakami, Y. Takasu, *J. Appl. Electrochem*., 2006, **36**, 1117.

20. Q. Yuan, Z. Zhou, J. Zhuang, X. Wang, *Chem. Mater*., 2010, **22**, 2395.

21. R.T.S. Oliveira, M.C. Santos, P.A.P. Nascent, L.O.S Bulhoes, E.C. Pereira, *Int. J. Electrochem. Sci*., 2008, **3**, 970.

22. K.W. Park, J.H. Choi, S.A. Lee, C. Pak, H. Chang, Y.E. Sung, *J. Catal*., 2001, **224**, 236.

23. K.W. Park, D.S. Han, Y.E. Sung, *J. Power Sources*, 2006, **163**, 82.

24. V.D. Noto, E. Negro, *J. Power Sources*, 2010, **195**, 638.

25. D. Friebel, D.J. Miller, D. Nordlund, H. Ogasawara, A. Nilsson, *Angew. Chem. Int. Ed*., 2011, **50**, 10190.

26. A. Baraldi, L. Bianchettin, S. de Gironcoli, E. Vesselli, S. Lizzit, L. Petaccia, G. Comelli, R. Rosei, *J. Phys. Chem. C*, 2011, **115**, 3378.

27. K. Yuge, T. Ichikawa, J. Kawai, *Mater. Trans*., 2010, **51**, 321.

28. P.D. Tran, S.Y. Chiam, P.P. Boix, Y. Ren, S.S. Pramana, J. Fize, V. Artero, J. Barber, *Energy Environ. Sci*., 2013, **6**, 2452.

29. Y. Zhang, M. Janyasupab, C.W. Liu, X. Li, J. Xu, C. Liu, *Adv. Funct. Mater*. 2012, **22**, 3570.

30. K. Mohanraju, L. Cindrella, *RSC Adv*., 2014, **4**, 11939.

31. Q. He, X. Yang, W. Chen, S. Mukerjee, B. Koel, S. Chen, *Phys. Chem. Chem. Phys*., 2010, **12**, 12544.

32. W. Sheng, S. Chen, E. Vescovo, Y.S. Horn, *J. Electrochem. Soc*., 2012, **159**, B96.

33. H.A. Gasteiger, S.S. Kocha, B. Sompalli, F.T. Wagner, *Appl. Catal. B*, 2005, **56**, 9.

34. W. Sheng, H.A. Gasteiger, Y.S. Horn, *J. Electrochem. Soc*., 2010, **157**, B1529.

35. X.Q. Gong, Z.P. Liu, R. Raval, P. Hu, P, *J. Am. Chem. Soc*., 2004, **126**, 8-9.

36. V.A. Sethuraman, J.W. Weidner, A.T. Haug, M. Pemberton, L.V. Protsailo, *Electrochim. Acta*, 2009, **54**, 5571.

37. N.M. Markovic, H.A. Gasteiger, P.N. Ross, *J. Phys. Chem*., 1995, **99**, 3411.

38. J.C. Meier, C. Galeano, I. Katsounaros, A.A. Topalov, A. Kostka, F. Schuth, K.J.J. Mayrhofer, *ACS Catal*., 2012, **2**, 832.

39. B.Y. Xia, W.T. Ng, H.B. Wu, X. Wang, X.W. Lou, *Angew. Chem. Int. Ed*., 2012, **51**, 1.

40. R. Loukrakpam, B.N. Wanjala, J. Yin, B. Fang, J. Luo, M. Shao, L. Protsailo, T. Kawamura, Y. Chen, V. Petkov, C.J. Zhong, *ACS Catal*., 2011, **1**, 562.

41. B. Lim, M. Jiang, P.H.C. Camargo, E.C. Cho, J. Tao, X. Lu, Y. Zhu, Y. Xia, *Science*, 2009, **324**, 1302.

42. C. Koenigsmann, A.C. Santulli, K. Gong, M.B. Vukmirovic, W.-ping Zhou, E. Sutter, S.S. Wong, R.R. Adzic, *J. Am. Chem. Soc*., 2011, **133**, 9783.

43. B.N. Wanjala, R. Loukrakpam, J. Luo, P.N. Njoki, D. Mott, C.J. Zhong, M. Shao, L. Protsailo, T. Kawamura, *J. Phys. Chem. C*, 2010, **114**, 17580.

44. F. Takasaki, S. Matsuie, Y. Takabatake, Z. Noda, A. Hayashi, Y. Shiratori, K. Ito, K. Sasaki, J. Electrochem. Soc., 2011, **158**, B1270.

45. F. Hasche, M. Oezaslan, P. Strasser, J. Electrochem. Soc., 2012, **159**, B24.

46. S. Alayoglu, B. Eichhorn, J. Am. Chem. Soc., 2008, **130**, 17479.

47. J.A. Rodriguez, D. Wayne Goodman, *J. Phys. Chem*., 1991, **95**, 4196.

48. H.L. Jiang, Q. Xu, *J. Mater. Chem*., 2011, **21**, 13705.

Figure Captions

Fig. 1 Powder XRD patterns of supportless and carbon supported Pt_3Rh nanoclusters.

Fig. 2 TEM images (a & b) and (c) HRTEM image of supportless Pt_3Rh nanocluster with corresponding (d) histogram.

Fig. 3 Cyclic voltammograms of supportless Pt_3Rh and Pt_3Rh/VC in N_2 saturated 0.5 M H_2SO_4 at a scan rate of 0.1 V s^{-1} at 25 °C.

Fig. 4 (a) Linear scan voltammograms and (b) K-L plots of SL Pt_3Rh and Pt_3Rh /VC nanoclusters in O_2 saturated 0.5 M H_2SO_4 at a scan rate of 0.01 V s^{-1} at 25 °C.

Fig. 5 ADT (a) CVs, (b) LSVs of SL Pt_3Rh at 2400 rpm and (c) normalized ORR current density of supportless and VC supported Pt_3Rh nanoclusters recorded at different potential cycling during ADT.

Fig. 6 TEM images and its corresponding histograms of supportless Pt_3Rh nanoclusters (a & C) before and (b & d) after ADT potential cycling (15,000 potential cycles).

Fig. 7 (a) CVs and (b) LSVs of SL Pt@Pt_3Rh nanoclusters recorded at different potential cycling during ADT.

Fig. 1

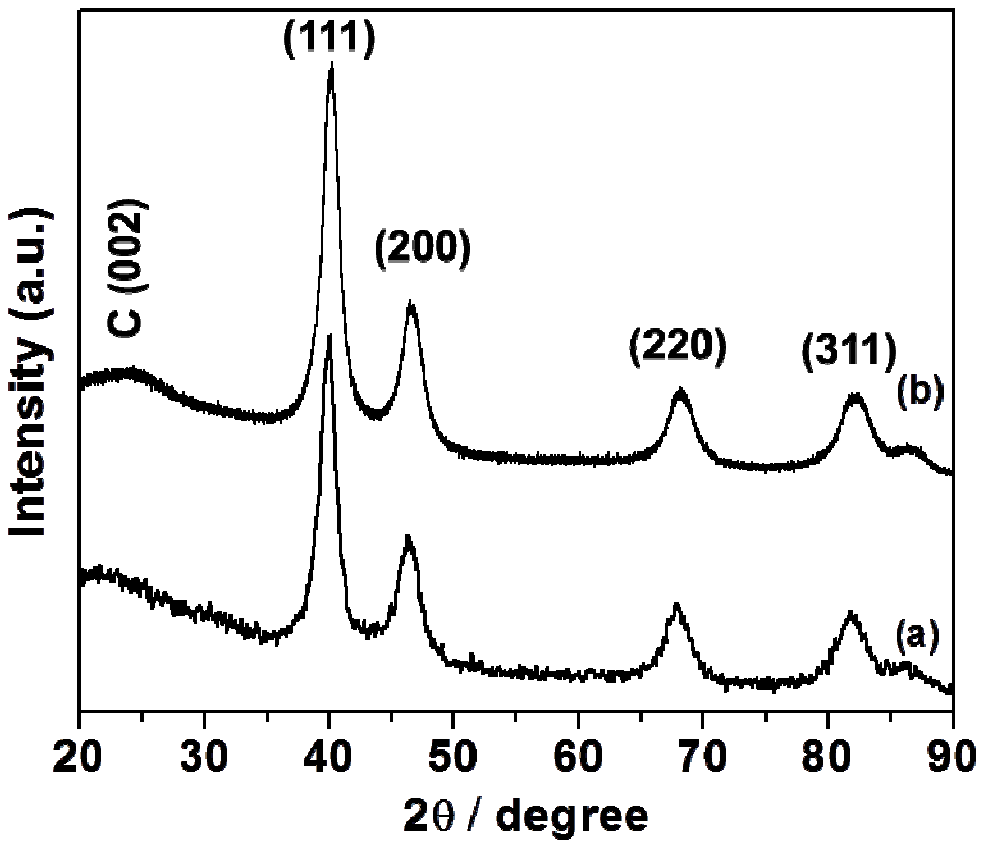

Fig. 2

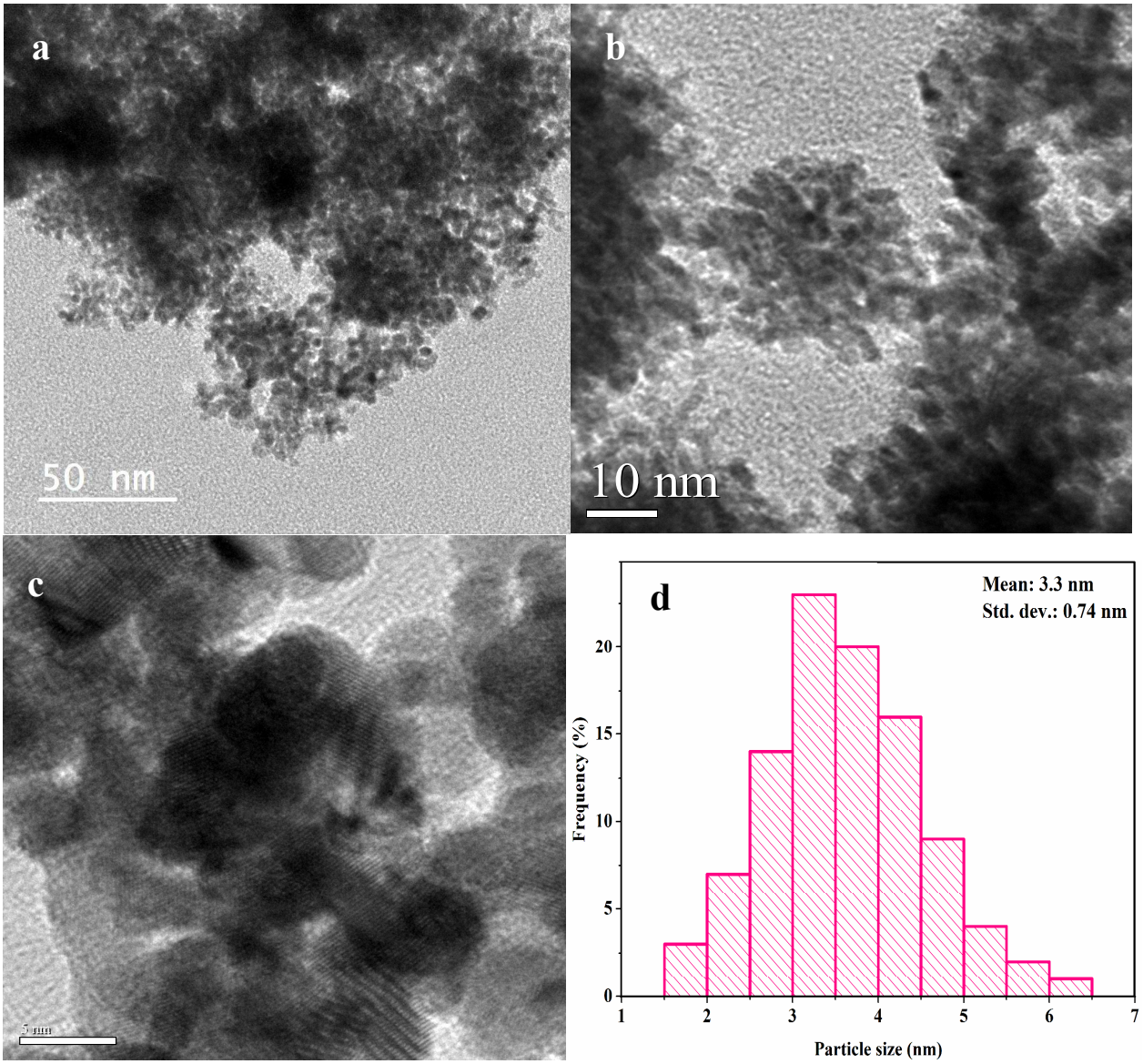

Fig. 3

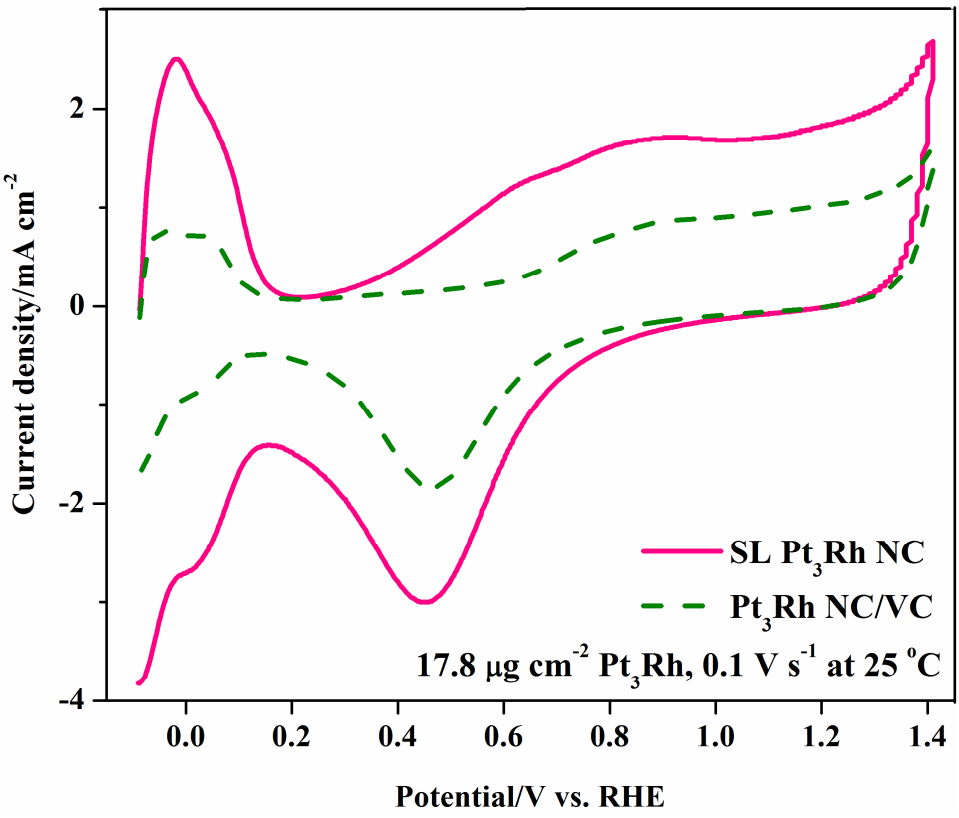

Fig. 4

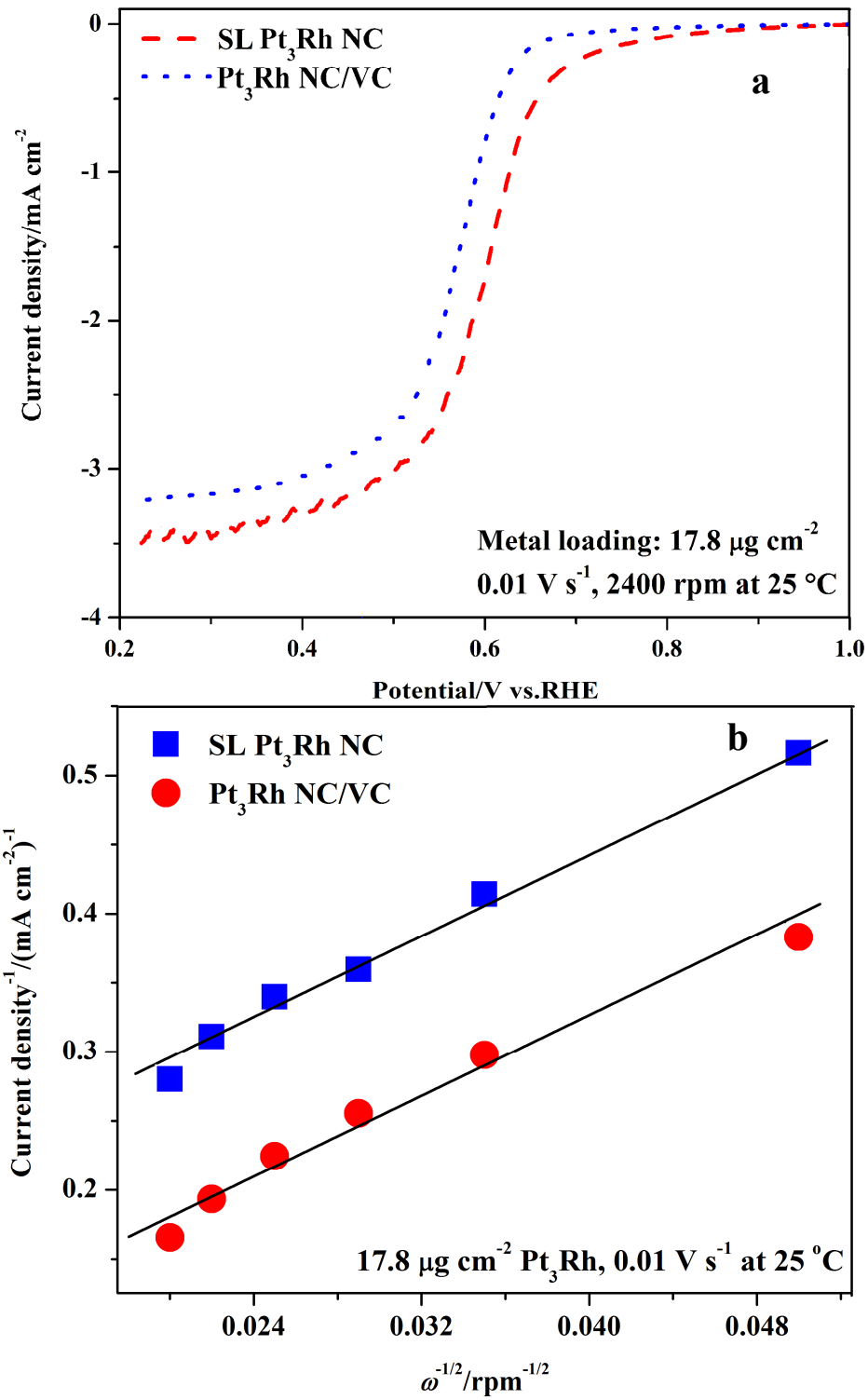

Fig. 5

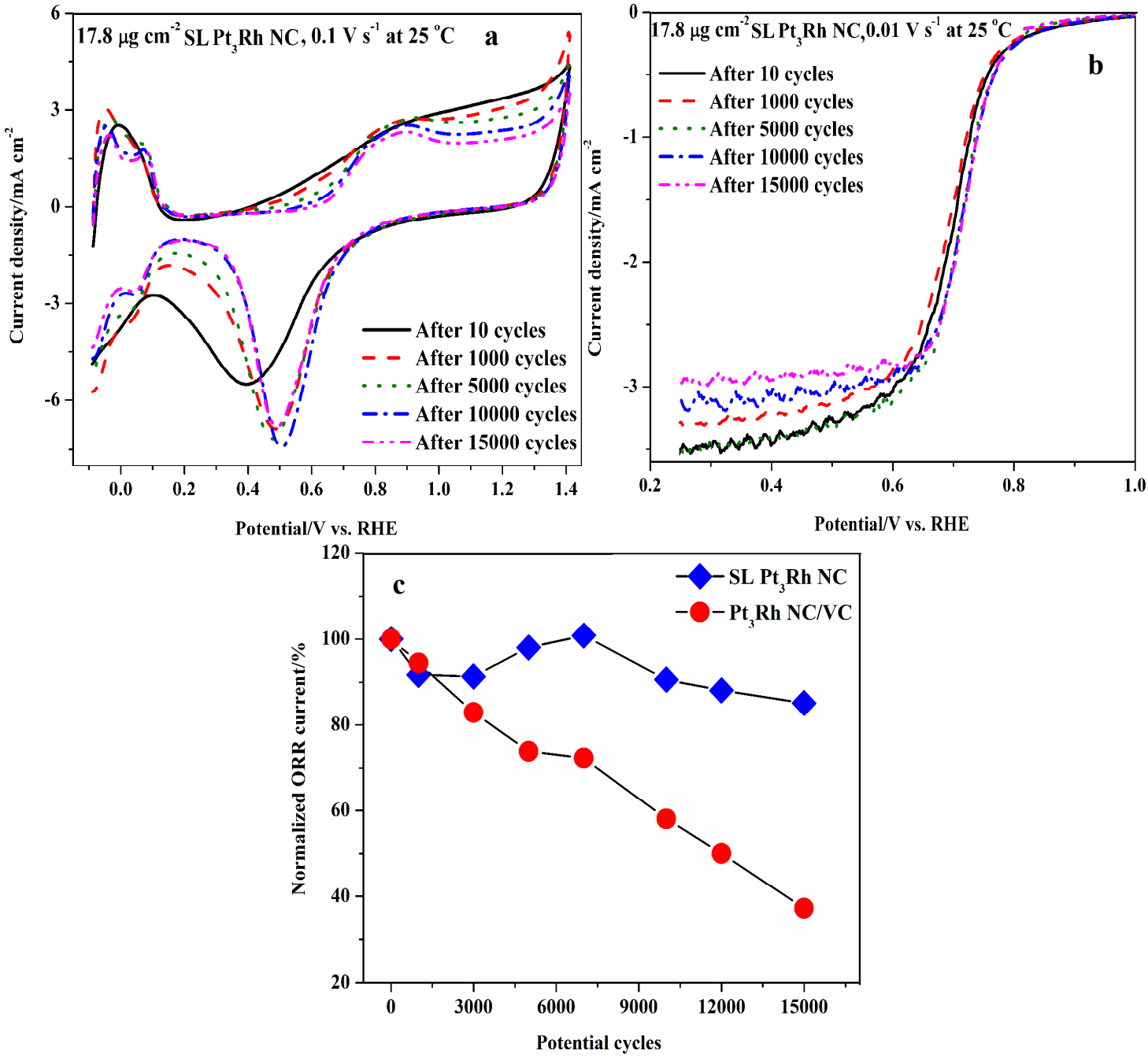

Fig. 6

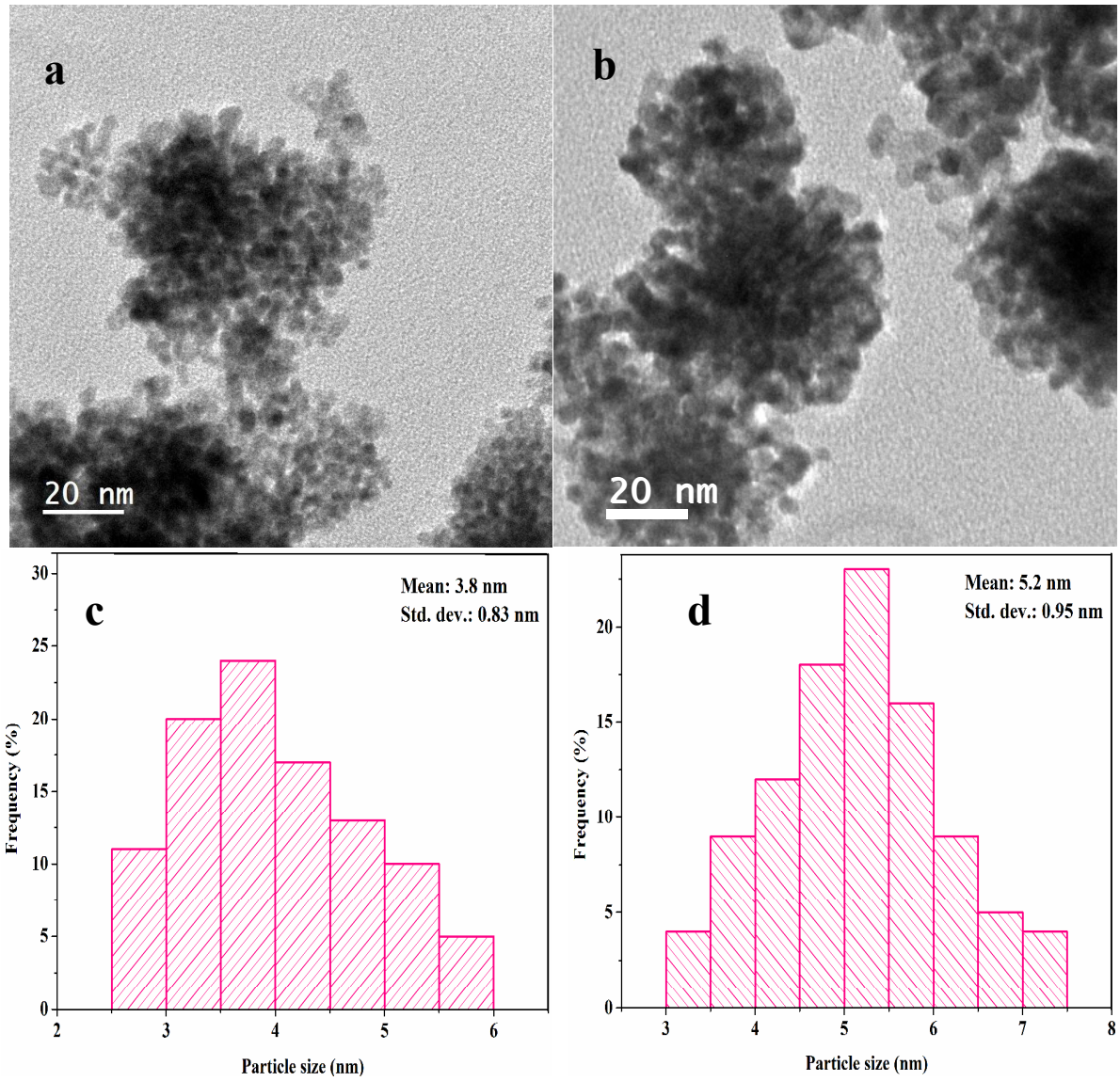

Fig. 7

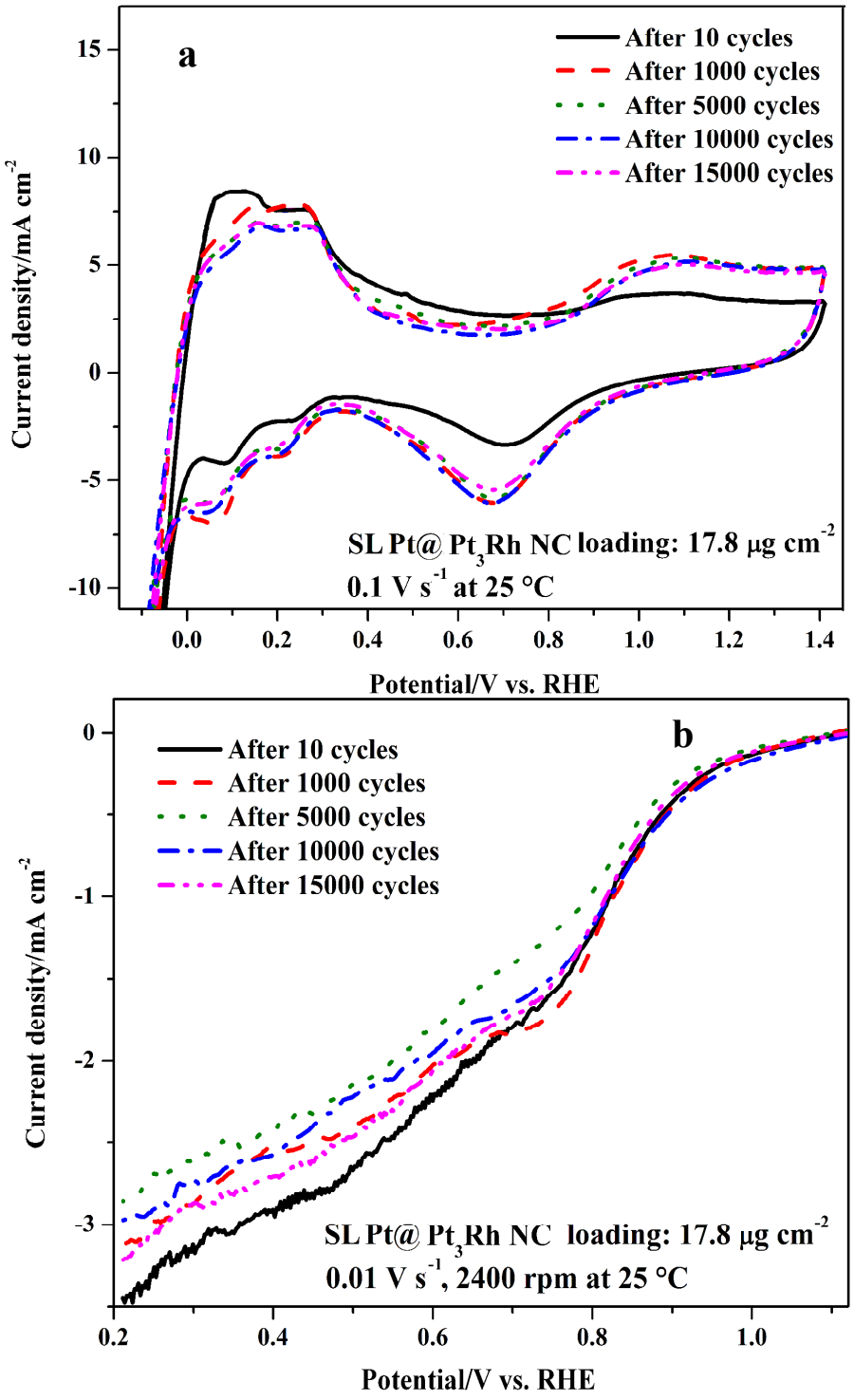

Table Captions

Table 1 Summary of ORR kinetic parameters for supportless and VC supported Pt_3Rh nanoclusters at 25 °C.

Table 2 Comparison of durability of Pt_3Rh nanocluster electrocatalysts with Pt based nanostructures from various literature reports.

Table 1

Catalyst	j_d (mA cm^{-2})	On set potential (V)	$E_{1/2}$ (V)	j_k (mA cm^{-2})	10^3 k (cm s^{-1})	b (mV dec^{-1})	α	10^6 i_0 (A cm^{-2})	n	MA (mA µg^{-1})
SL Pt_3Rh	3.50	0.78	0.59	0.08	3.50	115	0.52	0.96	4.0	0.0025
Pt_3Rh/VC	3.34	0.74	0.52	0.01	3.25	109	0.55	0.32	3.5	0.0001

j_d-limiting current density; $E_{1/2}$-half-wave potential; j_k-kinetic current density; b-Tafel slope; α-electron transfer coefficient; i_0-exchange current density; n-number of electron transfer; MA-mass activity @ 0.9 V.

Table 2

Ref. No.	Catalyst	Loading ($\mu g/cm^2$)	ECSA (m^2/g)	Loss of ECSA after ADT (%) / PC	ORR current density loss (%) / PC
37	Pt/C	11	71.0	74/10800	-NA-
38	Self supported Pt NAs	-	40.8	27.5/10000	-NA-
39	$Pt_{65}Ir_{11}Co_{24}/C$	16	70	85 90 70/20000	-NA-
41	Pd-Pt ND	15.3	48.5	50/10000	-NA-
42	Pt-Pd NW/C HP Pt/C	-	0.45 cm^2	37& 50/15000	~3 % with 15 mV degradation/15000
43	$Pt_{36}Ni_{15}Co_{49}/C$	6.6	56.6	28/10000	-NA-
44	Pt/Vulcan	51.9	~43.0	80.3/10000	-NA-
45	Pt/Vulcan XC 72R	23.8	47.0	19.1/10000	-NA-
Present study	**SL Pt@Pt_3Rh**	**17.8**	**214.3**	**7.8 % increase/15000**	**10.2/15000**
	SL Pt_3Rh NC		**154.4**	**9.1 % increase /15000**	**14.9/15000**
	Pt_3Rh NC/VC		**63.1**	**91.5/15000**	**60.6/1500**

NA-nanoassembly; ND-nanodentrites; NW-nanowires; NC-nanoclusters; HP-hollow porous; PC-potential cycles.